Materials Research Bulletin 46 (2011) 1403–1408

Contents lists available at ScienceDirect

Materials Research Bulletin

journal homepage: www.elsevier.com/locate/matresbu

Self-assembly of diverse alumina architectures and their morphology-dependent wettability

Lujun Yao [a], Maojun Zheng [a,*], Li Ma [b], Wei Li [b], Mei Li [b], Wenzhong Shen [a]

[a] *Laboratory of Condensed Matter Spectroscopy and Opto-Electronic Physics, and Key Laboratory of Artificial Structures and Quantum Control (Ministry of Education), Department of Physics, Shanghai Jiao Tong University, Shanghai, 200240, People's Republic of China*

[b] *School of Chemistry & Chemical Technology, Shanghai Jiao Tong University, Shanghai, 200240, People's Republic of China*

ARTICLE INFO

Article history:
Received 8 December 2010
Received in revised form 9 March 2011
Accepted 13 May 2011
Available online 20 May 2011

Keywords:
A. Nanostructures
A. Interfaces
B. Chemical synthesis
D. Surface properties

ABSTRACT

This work reports the fabrication of diverse nanostructured alumina films under high-field anodization in oxalic-acid electrolytes. Different surface morphologies of these alumina films can be obtained by adjusting reaction parameters, which was ascribed to the anisotropic chemical etching induced by the reaction heat and the concentration gradient of the oxalic-acid solution along the nanopore channels during the high-field anodization process. These alumina surfaces without coating low energy materials show remarkable morphology-dependent wettability. Specially, the alumina surface consisting of porous underlayer and nanowire pyramids with no chemical modification reveals excellent super water-repellent behavior for the first time. This study could provide a new approach for designing functional surfaces with tunable wettability.

1. Introduction

In natural world, many distinctive behavior characteristics of plant and animal kingdom are closely related to their special surface structures, such as hierarchical micro- and nanofibrillar morphologies on the superhydrophobic surface of lotus leaf and water strider' legs [1,2], which has inspired tremendous scientific interest. It has been understood that high surface roughness with hierarchical structure at both the micro- and nanoscale together with a low surface energy of the material are the key factor to superhydrophobicity [3–5]. The artificial superhydrophobic surfaces possessing high water contact angle (CA) and low adhesion have attracted much more attention because of their wide application ranges in functional microfluidics devices, water-proof or self-cleaning surfaces of high-quality products. In recent years, various approaches have been explored to manufacture roughness in dual-length-scale, such as electrospinning, layer-by-layer assembly, solution-immersion method, and template-based extrusion technique [6–9].

Since Masuda and Fukuda's study of self-ordered porous alumina film by a two-step replicating process [10], electrochemically produced porous anodized alumina (PAA) film has became one of the most common nanotemplates for preparation of one dimensional nanomaterials with electronic, magnetic and photonic properties [11–16]. Due to the attractive feature for its self-ordered hexagonal nanopore structure and low-cost processing, it also has been widely used as humidity sensors [17], filters [18] and the two-dimensional photonic crystals [19]. However, lots of other nanostructured alumina surfaces including nanotips, nanowire arrays or nanowire pyramids [20–22] were also prepared on porous alumina layers in the past years, and the researches on their wetting behavior have been developed. Those nanostructured alumina surfaces were mainly achieved via chemical acid etching of porous anodized alumina, and their superhydrophobic surfaces were realized by coating low surface energy materials, such as peruoro compounds and silicones [23–25].

In this paper, only the electrochemical anodization was employed to fabricate diverse nanostructured alumina surfaces in oxalic-acid electrolyte under high field. The high-field anodization is more efficient and can generate a larger interpore distance of PAA films, and a great deal of heat yielded during the anodization process is beneficial to the self-assembly of diverse alumina structure. Wetting behavior could be altered within ranges from Wenzel to Cassie states by changing surface morphologies. Particularly, the unmodified alumina surface consisting of porous underlayer and nanowire pyramids demonstrates both superhydrophobicity and superoleophilicity, which would be used in self-cleaning functions, separation of water and oil, and other applicable fields. The physical essence of the morphology-dependent wettability has been systematically analyzed.

---

[*] Corresponding author. Tel.: +86 021 54743242; fax: +86 021 54741040.
E-mail address: mjzheng@sjtu.edu.cn (M. Zheng).

0025-5408/$ – see front matter © 2011 Elsevier Ltd. All rights reserved.
doi:10.1016/j.materresbull.2011.05.018

2. Experimental

2.1. Preparation of diverse alumina architectures

Round aluminum slice (99.999% purity, 0.25 mm thickness) was cleaned ultrasonically with acetone and ethanol to get rid of grease in sequence, washed in deionized water and put into a tailor-made holder with a circular area of 2 cm^2 exposed to electrolytes. Aluminum slice was firstly electropolished using a constant voltage of 10 V in a 1:4 volume mixture (5 °C) of perchloric acid and ethanol for 5 min to improve surface smoothness before anodization. Two-step electrochemical anodization was applied for the fabrication, which has been described everywhere [10,17,20,21]. A large glass beaker (2 L), a powerful low-constant temperature bath and a vigorous stirrer (400 rpm) were employed to maintain low temperatures required for the high-field anodization, a graphite plate was used as cathode. Anodization was then carried out in a $C_2H_2O_4$–H_2O–C_2H_5OH electrolyte system ($C_2H_2O_4$, 0.3 M) at 120 V. In detail, the first anodization lasted for 5 min to form regular hexagonal nanopore arrays, then the foils were immersed in a mixture of 6 wt% phosphoric acid and 1.8 wt% chromic acid at a temperature of 60 °C for proper time to dissolve the orderless surfaces. Subsequently, the second anodization was conducted with some changed parameters in order to obtain diverse nanostructured alumina surfaces, as follows: (a) $t = 3$ min, $T = -8$ °C (sample A), (b) $t = 3$ min, $T = 0$ °C (sample B), (c) $t = 5$ min, $T = 0$ °C (sample C) and (d) $t = 8$ min, $T = 0$ °C (sample D). All the obtained samples were put into vacuum glove box to avoid contamination.

2.2. Characterization

The surface morphologies were observed by a field-emission scanning electron microscope (FE-SEM, Philips Sirion 200), and energy-dispersive X-ray (EDX) microanalysis was applied to investigate the chemical composition of the as-grown samples. CA and sliding angle of water droplet were measured using an optical contact-angle meter system (Data Physics Instrument GmbH, Germany) at ambient temperature.

3. Results and discussion

Fig. 1 is the top-view FE-SEM images of diverse alumina films fabricated in $H_2C_4O_2$–H_2O–C_2H_5OH system under appropriate anodizing parameters, exhibiting a dynamic evolution process of the surface morphologies from nanopores, nanotips, nanowire pyramids, and then to collapsed nanowire pyramids. Electrochemical anodization of aluminum in the acidic electrolyte leads to the growth of oxide film according to the following electrochemical reactions [26–28]:

Cathode:

$$2H^+ + 2e \rightarrow H_2\uparrow$$

Anode:

$$Al - 3e \rightarrow Al^{3+}$$

$$2Al^{3+} + 3O^{2-} \rightarrow Al_2O_3$$

The morphology and growth mechanism of PAA films on aluminum has been explained in detail in the former studies [26,29,30]. Fig. 1(a) shows the SEM image of sample A fabricated at -8 °C with anodization time of 3 min, the nanopore size is about 180 nm in average. Fig. 1(b) presents the large-scale nanotips formed on the surface of porous alumina layer by means of increasing electrolyte temperature. Former studies have revealed that chemical etching can happen in the oxalic-acid electrolyte with an increased temperature [13], and nanoporous surface will be etched into a desirable structures using 5% H_3PO_4 solution [21].

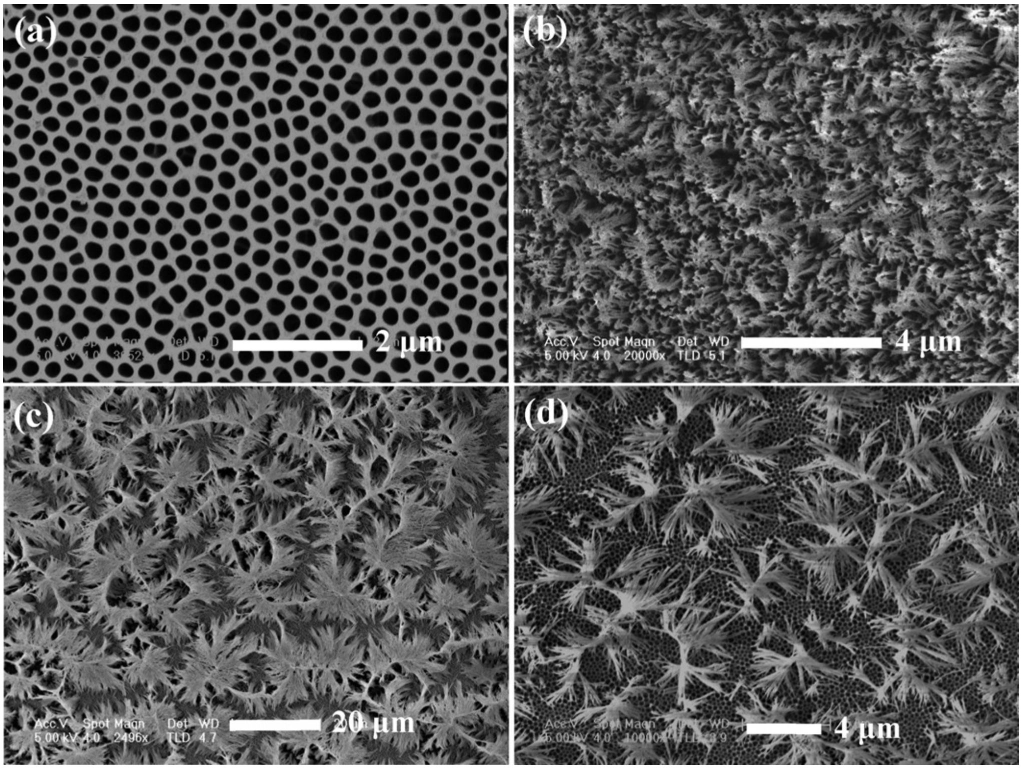

Fig. 1. Top-view FE-SEM images (a) sample A, PAA films; (b) sample B, alumina nanotips; (c) and (d) samples C and D, alumina nanowire pyramids with different sizes.

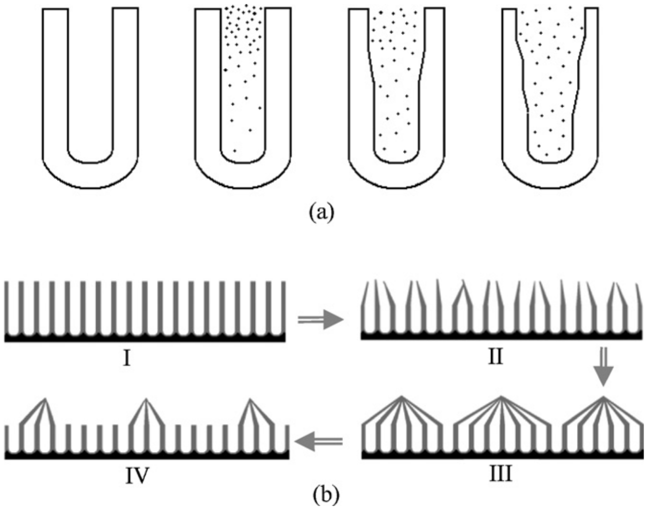

Fig. 2. (a) Sketches of the anisotropic etching characteristic for representing the formation of nanotips from segment by segment. The oxalic-acid concentration is higher on nanopore surfaces and then becomes nearly homogeneous with their size expanding. (b) Cross-sectional schematic diagram of the formation process of diverse alumina morphologies.

During the high-field anodization process, the anodization current density of sample B was observed to be as high as 4000 A/m^2 due to an increased electrolyte temperature from −8 °C to 0 °C, lots of heat yielded and could not diffuse immediately. The chemical etching process of alumina nanopores in oxalic-acid electrolyte was actuated by the yielded heat, which would not happen rapidly if a low-temperature electrolyte system or low-field anodization was supplied. However, it has been known that chemical acid etching of PAA films is anisotropic due to the inhomogeneous distribution of anion concentration in nanopore sidewalls and the concentration gradient of oxalic-acid solution along nanopore channels. Many research groups have confirmed that the nanopore sidewalls of PAA are composed of duplex oxide layers: an inner oxide layer with pure alumina and an outer oxide layer containing negative ion impurities [19], the outer oxide layer with anion-incorporated alumina is more prone to be etched under chemical acid etching process, but the locally dense regions are more resistant so that only alumina at the trigonal node left. On the other hand, the morphology evolution characteristic of nanotips can be attributed to the concentration gradient of the oxalic-acid solution along the nanopore channels. For a rapid supply rate, the concentration of oxalic-acid solution around PAA surface could be higher than that at the bottom of the nanopores, leading to the quicker dissolution of the porous alumina at the surface than that at the bottom [31]. Therefore, nanotips can form segment by segment with a smaller diameter at the top, the schematic diagram of anisotropic chemical acid etching process of PAA films in sequence is shown in Fig. 2(a). When the nanopore was widely expanded, the oxalic-acid concentration along nanopore channels became nearly homogeneous and the released heat was easily dissipated, which would slow down the oxalic-acid etching process. Fig. 1(c) presents a hierarchical alumina structure: a nanopore structural layer and nanowire pyramids at the surface. It has been revealed [21] that alumina nanowire pyramid is formed by the cells within the same ordered region. Self-ordering region of PAA films indicates that within the same region, the arrangement of the hexagonal cells is ordered. However, it is not ordered at the boundaries of these ordered regions due to the occurrence of defects or distortion in the pore sidewalls, then the alumina cells dissolved faster than those within the same ordered regions. Cells at the boundaries are totally dissolved while those within the ordered regions were partially dissolved, which induce the formation of alumina nanowires. These nanowires bent down and leant against each other to form nanowire pyramids due to the outer gravity field and the stirring influence. The nanowire pyramids of sample C with no obvious interspace could be directly attributed to the collapsed alumina nanowires formed by the further etching of nanotips (sample B). The size of each pyramid is about 10 μm in average, approximately equal to the size of an

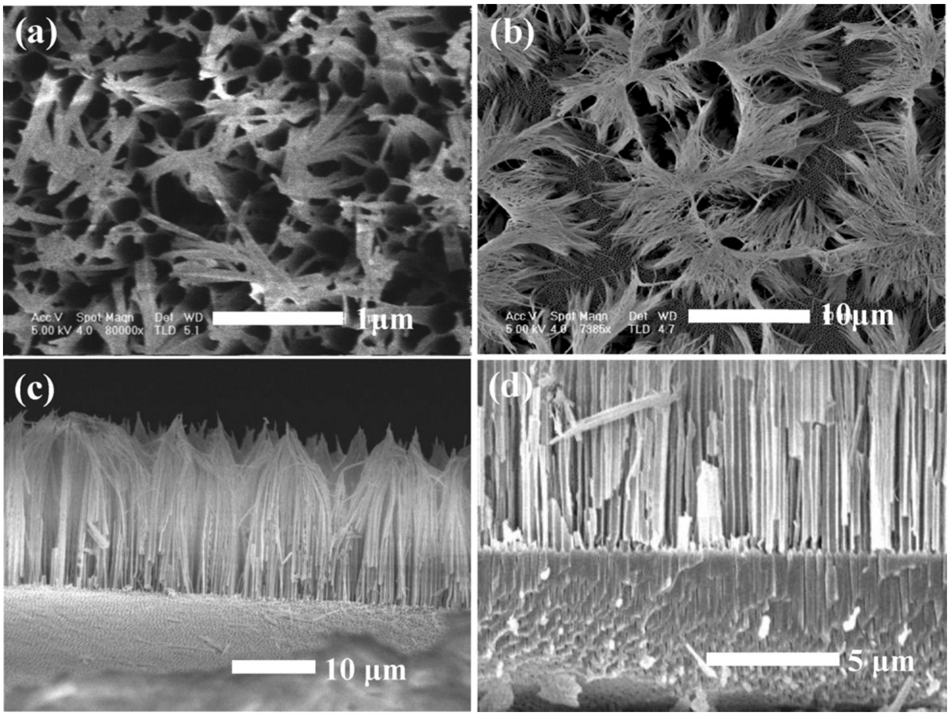

Fig. 3. (a) and (b) The corresponding high-magnification top-view FE-SEM images of samples B and C. (c) and (d) The low- and high-magnification cross-sectional FE-SEM images of sample C, an obvious interface was shown between the alumina porous layer in the below and the surface layer with alumina nanowires.

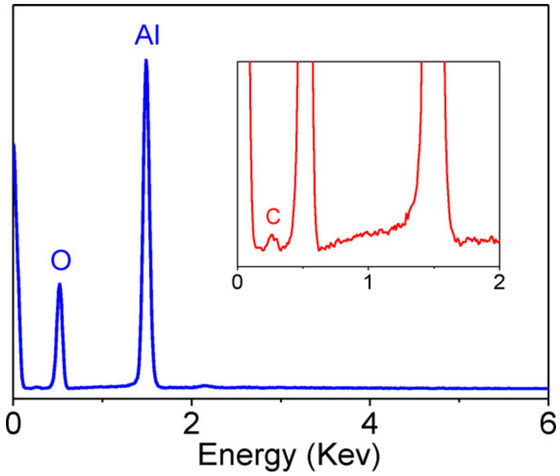

Fig. 4. EDX spectroscopy recorded on a selected area of sample C.

ordered region of PAA films. Fig. 1(d) shows the collapsed nanowire pyramids with small size ranging from 2 μm to 3 μm, and the interspace is 1 μm in average. Some of these nanowire pyramids nearly fell down. In this case, we suggested that alumina nanowire pyramids of sample D originated from those of sample C, which would be further etched and separated into two or three smaller pyramids with the high-field anodization processing. A cross-sectional schematic diagram describing the dynamic evolution of samples A, B, C and D are distinctly demonstrated in Fig. 2(b). It should be emphasized that it was the yielded heat which drove the formation of nanostructured alumina surfaces in oxalic-acid electrolyte, and some contrastive experimental results show that these alumina morphologies would not generated if the same temperature of −8 °C as the first anodization step or a higher stirring speed larger than 1000 rpm was used. Instead, only PAA films were obtained and their nanopore sizes might be a little larger. Therefore, heat-driven dissolution with anisotropic oxalic-acid etching characteristic was proposed for the nature of the self-assembly mechanism.

Fig. 3(a) and (b) is the high-magnification top-view FE-SEM images of samples B and C. All alumina nanopores were etched into nanotips with smaller diameters towards the tip, it is clearly seen that these nanotips stand on the porous layer (Fig. 3(a)). For sample C, the representative nanowire pyramids located on the surface of alumina nanoporous layer and consisted of large numbers of alumina nanowires. The typical cross-sectional FE-SEM images of sample C are demonstrated in Fig. 3(c) and (d), pyramidal structures were easily visible and there was an obvious interface between the alumina porous layer and the surface layer with destroyed nanopores (shown in Fig. 3(d)), illustrating that the oxalic-acid etching mainly happened on the nanopore surface of PAA films because of the anisotropic etching characteristic. Fig. 4 gives a representative chemical composition and stoichiometry through EDX spectroscopy recorded on a selected area of sample C, revealing that there were only Al, O and C elements existed in this nanostructured film, and C element with 7.48% atomic percent originated from the negative ion impurities $C_2O_4^{2-}$ that caused during the anodization process.

Surface wettability was evaluated by the CA measurement, as shown in Fig. 5. Contact angles of porous alumina films have been proved to be little influenced by the depth of nanopore when it become deeper than 1.7 μm [32], which was also checked by our experimental results. However, these alumina films prepared in our work were much larger than 1.7 μm, and their surface morphologies were considered as the only significant factor deciding CA values. Sample A shows hydrophilic property with CA of 71.6° in average, it should be proposed that the measured CA value is not stable until the time is upto 15 s because of the existed capillary force. Lots of tiny air bubbles were carefully observed when a water droplet was placed on sample A, revealing the penetrating of water into nanopores. For a compact flat alumina surface with no nanopores, CA is shown to be about 85°, less hydrophilic than sample A. According to the two classical wetting model, hydrophilicity of a rough surface increases in the Wenzel state for the primary hydrophilic surfaces. Therefore, wetting state on sample A should be Wenzel state, water wets the porous alumina surface and penetrates into each nanopore which has been directly verified based on the production of air bubbles from

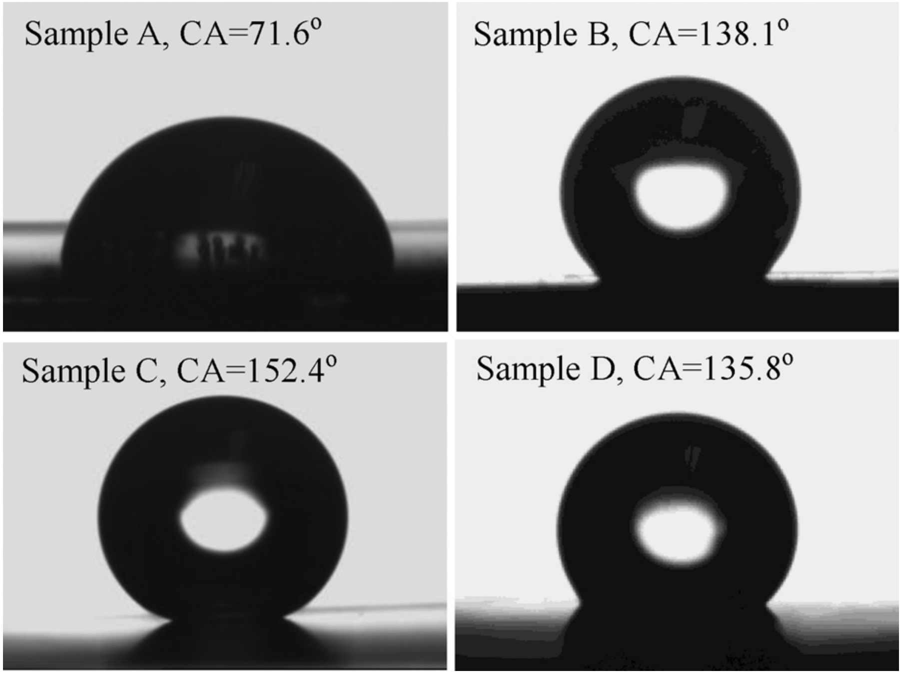

Fig. 5. The water CA photographs of samples A, B, C and D.

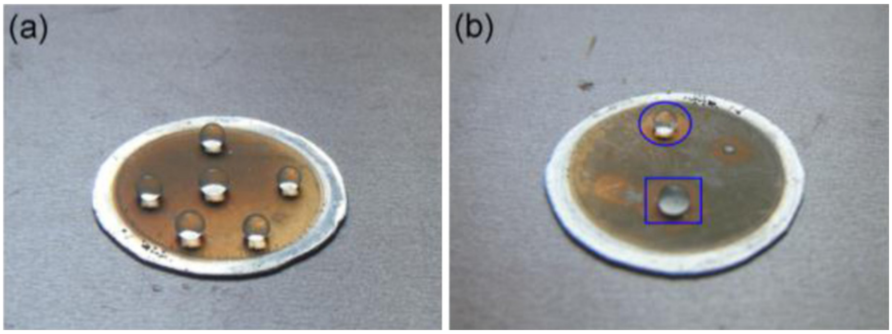

Fig. 6. (a) Photograph of six water droplets with nearly spherical shape located on the surface of sample C. (b) The phenomenon of automatically repelling water which is from instantaneous ice melting.

the nanochannels. Sample B with alumina nanotips on the surface presents hydrophobicity with CA of 138.1°, and shows no air bubble phenomenon. When a water droplet was placed on the surface of sample B, it possibly stood on this tip-like nanostructured surface rather than permeating into alumina nanochannels. The contact way between water droplet and the nanostructured surface changed from "area-contact" (sample A) to "point-contact" (sample B), so it can make a higher fraction of air/water and then leads to the increase of CA value. The corresponding water CA on a hierarchical surface of sample C (Fig. 1(c)) was measured to be 152.4° in average, a typical CA photograph is shown in Fig. 5. It was obvious when the deionized water droplet about 5 μl was placed on its surface, it yielded a nearly spherical droplet at the microscopic level. We notice that the superhydrophobic surface exhibits a stable character in air with the CA showing no apparent change, and the water droplet eventually evaporates on the surface of alumina nanowire pyramids. The previous studies have demonstrated that the fractal geometry created by nanostructures on microstructures become a novel approach to construct superhydrophobic surfaces as the famous lotus leaf in the natural world. Accordingly, the surface of sample C has the same fractal geometry as lotus leaf, the micron-sized alumina pyramids liked the papillae of lotus leaf and their further component alumina nanowires could be considered as the branch-like nanostructures of lotus leaf. This micro- and nanoscale hierarchical structures bring a large contact area between the air trapped within alumina films and water droplet, which is essential for obtaining superhydrophobic surface. Sample D presents a lower CA of 135.8°, a remarkable distinction from the morphology of sample C is the smaller size of the nanowire pyramids with a little tilted or collapsed construction, which decreases the fraction of air/water. On the other hand, water droplet possibly touches the porous alumina layer which may cause CA decrease due to the capillary force. The above discussion indicates that rational fabrication of alumina nanowire pyramids with well-controlled size and interspace will be an effective approach to realize the well superhydrophobic performance.

The sliding angle which reflects the relationship between advancing and receding contact angles was measured by tilting the sample platform of OCA contact angle system until the water droplet rolled off the fixed sample C. A water droplet easily slides off its surface when the inclination angle exceeds 9.4°. Fig. 6(a) shows a typical photograph of sample C with six perfect and nearly spherical water droplet standing upon it, it's noted that water droplets are hardly able to stick, providing further evidence for its super water-repellent properties. The lower sliding angle can be attributed to the existed interspace between nanowire pyramids which induced the discrete contact line around water droplets, consequently resulting in the drastic decrease of sliding angles [33]. This super water-repellent property could be useful in practical needs such as self-cleaning function and drag-reduction. Automatically repelling water which is from instantaneous ice melting is further demonstrated in Fig. 6(b). In detail, tiny ice blocks with arbitrary shape were placed on the surface of sample C with room temperature, it was interesting to find that the molten ice block fast agglomerated to form a nearly spherical water droplet. The water droplets signed in circular loop and quadrate loop are corresponding to the total and partial molten ice block, the automatic contraction phenomenon was obvious. Moreover, the unmodified super water-repellent alumina surface is also superoleophilic. When a diesel oil droplet (~5 μl) was dropped on the surface, it rapidly spread over the micro- and nanostructured surface with CA value nearly equal to 0°, which was different from previous superhydrophobic surfaces of alumina with post-modification using low energy hydrophobic materials [23–25]. The unique alumina surface demonstrating both superhydrophobic and superoleophilic properties has, to our knowledge, not been reported to date.

4. Conclusion

The self-assembly of diverse nanostructured alumina films has been realized under high-field anodization in oxalic-acid electrolyte by adjusting anodization parameters. Morphology-dependent wettability has been observed on the nanostructured alumina films. The heat-driven anisotropic chemical etching model was introduced for explaining the formation of different surface morphologies on the films. Specially, the self-assembled hierarchical alumina surfaces exhibit excellent anti-adhesion to water droplets, automatically repelling water and superoleophilic properties. To our knowledge, it's the first time to prepare superhydrophobic surface of alumina films with no organic modification. It has advantages over the application in high temperature ambient and could be applicable in self-cleaning, functional separation and filtration equipment.

Acknowledgments

This work was supported by the Natural Science Foundation of China (grant nos. 10874115 and 10734020), National Major Basic Research Project of 2010CB933702, Shanghai Nanotechnology Research Project of 0952nm01900, Shanghai Key Basic Research Project of 08JC1411000, and Research fund for the Doctoral Program of Higher Education of Chain.

References

[1] T.L. Sun, L. Feng, X.F. Gao, L. Jiang, Acc. Chem. Res. 38 (2005) 644.
[2] X.F. Gao, L. Jiang, Nature 432 (2004) 36.
[3] M. Piech, T.L. Sounart, J. Liu, J. Phys. Chem. C 112 (2008) 20398.
[4] H.I. Hsiang, M.T. Liang, H.C. Huang, F.S. Yen, Mater. Res. Bull. 42 (2007) 420.
[5] C. Badre, T. Pauporté, M. Turmine, D. Lincot, Nanotechnology 18 (2007) 365705.

[6] M. Ma, R.M. Hill, J.L. Lowery, S.V. Fridrikh, G.C. Rutledge, Langmuir 21 (2005) 5549.
[7] L. Zhai, F.C. Cebeci, R.E. Cohen, M.F. Rubner, Nano Lett. 4 (2004) 1349.
[8] S.T. Wang, L. Feng, L. Jiang, Adv. Mater. 18 (2006) 767.
[9] L. Feng, S.H. Li, H.J. Li, J. Zhai, Y.L. Song, L. Jiang, D.B. Zhu, Angew. Chem. Int. Ed. 41 (2002) 1743.
[10] H. Masuda, K. Fukuda, Science 268 (1995) 1466.
[11] J.X. Xu, X.M. Huang, G.Z. Xie, Y.H. Fang, D.Z. Liu, Mater. Res. Bull. 39 (2004) 811.
[12] K. Biswas, Y. Qin, M. DaSilva, R. Reifenberger, T. Sands, Phys. Status Solidi (a) 204 (2007) 3153.
[13] K. Nielsch, F. Müller, A.-P. Li, U. Gösele, Adv. Mater. 12 (2000) 582.
[14] G.B. Yue, Q.L. Xu, G.W. Meng, X.L. He, F.M. Han, L.D. Zhang, J. Alloys Compd. 477 (2009) L30.
[15] K. Nishio, H. Masuda, Electrochem. Solid-State Lett. 7 (2004) H27.
[16] X.Y. Zhang, L.H. Xu, J.Y. Dai, Y. Cai, N. Wang, Mater. Res. Bull. 41 (2006) 1729.
[17] L.J. Yao, M.J. Zheng, H.B. Li, L. Ma, W.Z. Shen, Nanotechnology 20 (2009) 395501.
[18] T. Kyotani, W.H. Xu, Y. Yokoyama, J. Inahara, H. Touhara, A. Tomita, J. Membr. Sci. 196 (2002) 231.
[19] J. Choi, Y. Luo, R.B. Wehrspohn, R. Hillebrand, J. Schilling, U. Gösele, J. Appl. Phys. 94 (2003) 4757.
[20] Q.W. Sun, G.Q. Ding, Y.B. Li, M.J. Zheng, W.Z. Shen, Nanotechnology 18 (2007) 215304.
[21] Y.B. Li, M.J. Zheng, L. Ma, M. Zhong, W.Z. Shen, Inorg. Chem. 47 (2008) 3140.
[22] Y.T. Tian, G.W. Meng, T. Gao, S.H. Sun, T. Xie, X.S. Peng, C.H. Ye, L.D. Zhang, Nanotechnology 15 (2004) 189.
[23] W.C. Wu, X.L. Wang, D.A. Wang, M. Chen, F. Zhou, W.M. Liu, Q.J. Xue, Chem. Commun. 1043 (2009).
[24] K. Tadanaga, N. Katata, T. Minami, J. Am. Ceram. Soc. 80 (1997) 1040.
[25] W. Lee, B.G. Park, D.H. Kim, D.J. Ahn, Y. Park, S.H. Lee, K.B. Lee, Langmuir 26 (2010) 1412.
[26] J.P. O'Sullivan, G.C. Wood, Proc. R. Soc. Lond. A 317 (1970) 511.
[27] C.H. Huang, L. Chen, C.L. Yang, Sep. Purif. Technol. 65 (2009) 137.
[28] V. Sadasivan, C.P. Richter, L. Menon, P.F. Williams, AICHE J. 51 (2005) 649.
[29] V.P. Parkhutik, V.I. Shershulsky, J. Phys. D: Appl. Phys. 25 (1992) 1258.
[30] O. Jessensky, F. Müller, U. Gösele, Appl. Phys. Lett. 72 (1998) 1173.
[31] L.F. Huang, M. Satio, M. Miyagi, K. Wada, Appl. Opt. 32 (1993) 2039.
[32] C.B. Ran, G.Q. Ding, W.C. Liu, Y. Deng, W.T. Hou, Langmuir 21 (2008) 9952.
[33] L. Feng, S.H. Li, Y.H. Li, H.J. Li, L.J. Zhang, J. Zhai, Y.L. Song, B.Q. Liu, L. Jiang, D.B. Zhu, Adv. Mater. 14 (2002) 1857.